Mechanics of Advanced Composite Structures

Journal homepage: https://macs.semnan.ac.ir/

Semnan University

ISSN: 2423-7043

Research Article

Development and Characterization of a High-Performance Polyurethane-Based Colored Pavement Binder Including Calcium Carbonate and Polyethylene Glycol for Improved Thermal and Mechanical Durability

Abbas Ghareghashi [a*], Mohammad Ali Torangi [b], Hossein Taghipoor [a]

[a] *Engineering Faculty, Velayat University, Iranshahr, 9917638733, Iran*

[b] *Faculty of Engineering, Golestan University, Gorgan, 4913815759, Iran*

ARTICLE INFO

Article history:

Received: 2024-10-19
Revised: 2025-03-22
Accepted: 2025-05-12

Keywords:

Polyurethane;
Colored pavement binder;
Calcium carbonate;
Polyethylene glycol (PEG);
Phase change material;
Thermal management;
Mechanical reinforcement;
Urban Heat Island.

ABSTRACT

This work presents the development of a high-performance colored polyurethane (PU)-based pavement binder, modified with calcium carbonate ($CaCO_3$) and polyethylene glycol (PEG-4000, molecular weight 4000 g·mol^{-1}), designed to simultaneously enhance mechanical strength and thermal regulation performance. A suite of formulations containing varying concentrations of PEG (0–10 wt.%) and $CaCO_3$ (0–20 wt.%) was synthesized and subjected to a dual-stage curing protocol to ensure full cross-linking. The FTIR and XRD analyses indicated the preservation of the crystalline phases of $CaCO_3$, the PEG confinement, and that PU was successfully crosslinked. The thermal characterization methods (DSC and TGA) showed that PEG imparted a latent heat storage capacity of around 87 J g^{-1}, while $CaCO_3$ improved thermal stability and increased residual mass during high-temperature exposure. Mechanical testing revealed a notable increase in tensile strength, rising from approximately 1.07 to 3.16 MPa, along with an elongation at break reaching around 276% in the optimized formulations. Measurements of surface temperature under simulated solar exposure showed a reduction of 8–10 °C compared to traditional asphalt. The results demonstrate the synergistic effect of $CaCO_3$ reinforcement and PEG-induced thermal buffering in an environmentally friendly pavement binder in environmentally friendly pavement binder, thermally adaptable, thereby ensuring long-term structural durability. These findings provide a practical framework for designing climate-adaptive pavement binders with improved long-term durability.

1. Introduction

The increasing demand for metropolitan road networks that can withstand heavy traffic, harsh temperatures, and long-term performance has spurred research on multifunctional pavement binders. Traditional asphalt binders are widely used, but they are sensitive to temperature, prone to fatigue and cracking, and lack surface thermal regulation, especially in warmer climates [1–4]. These limitations undermine durability and intensify the Urban Heat Island (UHI) effect, leading to elevated surface temperatures and faster material degradation. The developed

* **Corresponding author.**
E-mail address: A.Ghareghashi@velayat.ac.ir

Cite this article as:

Ghareghashi, A., Torangi, M. A. and Taghipoor, H., 2026. Development and Characterization of a High-Performance Polyurethane-based Colored Pavement Binder Including Calcium Carbonate and Polyethylene Glycol for Improved Thermal and Mechanical Durability. *Mechanics of Advanced Composite Structures*, 13(2), pp. xxx-xxx.

https://doi.org/10.22075/MACS.2025.39313.2050

binder is specifically designed for high-traffic metropolitan road networks in arid and semi-arid regions (hot climates). It targets a service temperature range where pavement surfaces frequently exceed 60 °C, corresponding to a Performance Grade (PG) of 76-22 or higher [5–8].

To tackle these challenges, extensive research has been conducted on polymer-modified asphalts using styrene-butadiene-styrene (SBS) or styrene-butadiene rubber (SBR). These materials demonstrate enhanced performance when exposed to high temperatures, exhibit superior rheological stability, and offer improved resistance to permanent deformation [2,6,8,9]. However, these modifiers do not consistently provide enduring mechanical strength and effective thermal management, particularly when exposed to prolonged sunlight in hot climates [9–11]. Therefore, advanced binder systems are required to improve mechanical performance while maintaining thermal stability.

Polyurethane (PU) has recently emerged as a viable binder or asphalt modifier owing to its adaptable chemical structure, improved mechanical strength, and ability to form dense cross-linked networks via isocyanate–polyol interactions [3,10,12–15]. PU-modified binders exhibit superior deformation resistance, enhanced durability under cyclic loading, and stick better to aggregates [3,10,13,15,16]. The polyurethane matrix facilitates the incorporation of functional additives without compromising the fundamental integrity of the polymer network [12,15,16]. Recent research into high-performance composites highlights that systematic filler content optimization is critical for tailoring the mechanical and barrier properties of the final matrix [17–19]. Furthermore, a comprehensive characterization framework—incorporating FTIR, XRD, and TGA—is essential to validate the successful chemical isolation and structural integration of these reinforcement phases into the host polymer [17,20]. Even with these benefits, unresolved questions remain regarding the multi-functional optimization of PU-based binders for diverse applications.

Few studies address dual-functional techniques that combine polymeric phase-change materials (PCMs) for heat control and inorganic fillers for structural reinforcement; most studies concentrate on mechanical or rheological improvement [13,21,22]. Despite possible synergistic effects on tensile strength, toughness, and surface temperature management, the integration of reinforcement and thermal buffering within a single PU network is still poorly understood. Furthermore, whereas PCMs and high-reflectivity colored asphalt have been demonstrated separately to lessen the impacts of UHI [6,7,23–28], their combined use in a PU matrix is rarely studied. Comprehensive studies connecting molecular structure, microstructural dispersion, and macro-scale thermal-mechanical performance are scarce, despite the fact that partial studies look at chemical structure (FTIR, XRD), microstructure (SEM), and thermal characteristics (DSC, TGA) [10,21,22,29].

In order to fill these gaps, this study creates a new colored PU-based binder that contains polyethylene glycol (PEG-4000) as a latent-heat PCM and calcium carbonate ($CaCO_3$) as a high-modulus mineral filler. In polymer composites, $CaCO_3$ is well known for its affordability, stiffness, and reinforcing effectiveness, which enhance modulus, the generation of heat residues, and mechanical durability [30–33]. Dynamic thermal buffering under solar exposure is made possible by PEG, a well-characterized PCM that offers latent heat storage through reversible solid-liquid transitions [28,34,35]. It is expected that the addition of PEG and $CaCO_3$ to a cross-linked PU network will result in synergistic advantages, including higher resistance to thermal and mechanical degradation, increased thermal capacity, and improved tensile strength and elongation. Unlike binary systems that focus solely on rheological improvement, this work investigates a ternary hybrid that simultaneously optimizes mechanical toughness and thermal regulation within a permanent thermoset network. This integration of molecular-scale PEG confinement and macro-scale mineral reinforcement bridges a significant gap in current climate-adaptive binder research.

The particular objectives are:

To synthesize and optimize colored PU-based binders using different amounts of PEG (0–10 wt.%) and $CaCO_3$ (0–20 wt.%) while methodically evaluating synergistic effects;

Characterize chemical structure, crystallinity, microstructure, thermal transitions, and decomposition behavior using FTIR, XRD, DSC, and TGA;

To quantify mechanical performance via tensile testing and assess surface cooling under simulated solar exposure;

To establish mechanistic correlations connecting molecular and microstructural attributes with macro-scale thermal and mechanical performance, thereby providing a scientific foundation for practical urban pavement applications.

By bridging these gaps, this study enhances understanding of multifunctional PU-based binders and proposes a viable solution for durable, climate-adaptive pavement systems capable of mitigating UHI effects and reducing maintenance requirements in hot climates.

2. Experimental Section

2.1.Materials

A two-component polyurethane (PU) system was employed as the main binding material. It consisted of a polyol prepolymer and an isocyanate-based hardener, both supplied by Epoxy Ran Co. (Tehran, Iran). Compared to traditional bitumen modifiers such as EVA or SBS, the resin was selected for its measured adhesion, rapid curing capability, and high cross-linking density.

Polyethylene glycol (PEG-4000), a semi-crystalline polymer with a molecular weight of 4000 g·mol^{-1}, was utilized as a phase-change additive to provide latent heat functionality. PEG-4000 was chosen because of its stable melting point of approximately 60°C and great compatibility with polyurethane matrices due to its hydroxyl end groups.

Calcium carbonate ($CaCO_3$) was incorporated as an inorganic mineral filler to enhance the stiffness, modulus, and thermal resistance of the binder. A fine-grade calcite powder (<5 μm particle size, purity >98%) was used.

To achieve desired reflectivity and color stability, an iron oxide red pigment (Fe_2O_3, particle size <1 μm) was introduced at 2–5 wt.%. This pigment has a proven capacity to increase albedo and mitigate heat absorption in colored pavement applications.

Additionally, minor amounts of aromatic oil were employed as a temporary plasticizer to reduce viscosity during mixing, and glycerin was included as a stabilizing additive to enhance interfacial compatibility between organic and inorganic components.

2.2. Formulation and Sample Preparation

The synthesis of PU-based colored pavement binders followed a controlled, multistage procedure designed to ensure optimal additive dispersion, consistent film properties, and complete curing.

Step 1 – Base Polymer Preparation

First, the polyol component of the PU system was incorporated into a high-shear mechanical mixer at 600 rpm. To simplify the processability, 2 wt.% aromatic oil was dispersed and stirred for 5 minutes at ambient temperature.

Step 2 – PEG Integration

PEG-4000 was preheated to 60 °C until melted and slowly homogenized to the polyol phase under constant stirring. The PEG fraction was varied between 0 and 10 wt.%, based on formulation design. The system was maintained at 60 °C for 15 min to promote partial hydrogen bonding and uniform mixing between polyol hydroxyl groups and PEG.

Step 3 – Filler Dispersion

$CaCO_3$ powder was gradually incorporated into the pre-mixed polyol–PEG solution at filler loadings of 0, 10, and 20 wt.%. The dispersion step was performed under vacuum mixing of –0.08 MPa to eliminate entrapped air bubbles and agglomerates. The viscosity of the mixture was carefully monitored to ensure uniform rheological consistency across samples.

Step 4 – Pigment Addition

Once the mixture became homogeneous, 3 wt.% iron oxide pigment was introduced at 45°C and mixed for 5 min at 800 rpm. The moderate temperature prevented any potential thermal degradation or discoloration of the pigment.

Step 5 – Curing and Casting

The reactive mixture was cast into precision-machined silicone molds specifically designed to yield ASTM D638 Type IV geometries. The use of flexible silicone molds ensured the production of specimens with high dimensional accuracy and smooth surfaces, minimizing edge defects that could act as stress concentrators during tensile loading. Finally, the isocyanate component was added to the polyol mixture in a stoichiometric NCO/OH ratio of approximately 1.05:1, ensuring full urethane network formation. The system was stirred rapidly (1000 rpm, 2 min) and poured into silicone molds of defined dimensions for subsequent testing. The reactive mixture was then cast into silicone molds of predefined dimensions.

The curing protocol involved:

Primary curing: 24 h at room temperature (25 ± 2°C)

Post-curing: 3 h at 60°C to ensure complete cross-linking and structural stabilization.

After curing, specimens were demolded and conditioned for 48 h in a desiccator before characterization.

A Schematic illustration of the preparation process for the polyurethane-based colored pavement binder is presented in Figure 1. Figure 1 not only illustrates the sequential preparation steps but also clarifies the integration pathway of PEG and $CaCO_3$ into the polyurethane matrix, which is critical for ensuring formulation reproducibility and controlled curing. It illustrates the primary polyurethane components, additives ($CaCO_3$, PEG-4000, and Fe_2O_3 pigment), and various stages of binder formulation and curing.

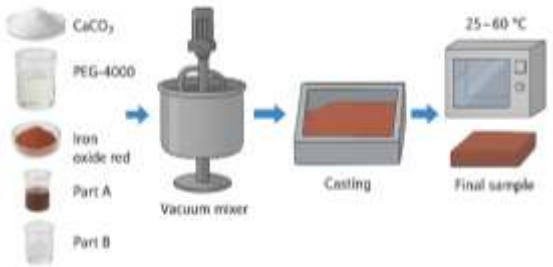

Fig. 1. Schematic illustration of the preparation procedure for the PU-based hybrid binder containing $CaCO_3$ and PEG-4000

2.3. Sample Coding and Composition

All synthesized samples were coded according to the relative content of PEG and $CaCO_3$. Table 1 lists the formulations and their corresponding designations. Table 1 provides the structural logic behind the sample coding system, enabling systematic comparison of additive concentration effects in the Results and Discussion section. Figure 2 illustrates the physical appearance of the prepared samples alongside their respective additive concentrations. Figure 2 visually confirms the uniform coloration and physical integrity of the cured binders, supporting the consistency of additive dispersion prior to mechanical and thermal evaluation.

Sample 1: Oil=5 wt.%, Filler= 1 wt.%, Polymer= 0.3 wt.%

Sample 2: Oil=5 wt.%, Filler= 1.5 wt.%, Polymer= 0.55 wt.%

Sample 3: Oil=5 wt.%, Filler= 2 wt.%, Polymer= 0.3 wt.%

Sample 4: Oil=6.5 wt.%, Filler= 1 wt.%, Polymer= 0.55 wt.%

Sample 5: Oil=6.5 wt.%, Filler= 1.5 wt.%, Polymer= 0.8 wt.%

Sample 6: Oil=6.5 wt.%, Filler= 1.5 wt.%, Polymer= 0.55 wt.%

Sample 7: Oil=6.5 wt.%, Filler= 1.5 wt.%, Polymer= 0.3 wt.%

Sample 8: Oil=6.5 wt.%, Filler= 2 wt.%, Polymer= 0.55 wt.%

Sample 9: Oil=8 wt.%, Filler= 1% wt.%, Polymer= 0.8 wt.%

Sample 10: Oil=8 wt.%, Filler= 1 wt.%, Polymer= 0.3 wt.%

Sample 11: Oil=8 wt.%, Filler= 2 wt.%, Polymer= 0.8 wt.%

Sample 12: Oil=8 wt.%, Filler= 2 wt.%, Polymer= 0.3 wt.%

(a)

(b)

Fig. 2. (a) Visual appearance of cured polyurethane-based colored pavement binders with varying concentrations of $CaCO_3$ and PEG-4000; (b) Photograph of the casting silicone mold and the prepared ASTM D638 Type IV tensile specimen demonstrating dimensional consistency.

Table 1. Composition of the PU-based binder formulations

Sample Code	$PEG\ (wt.\%)$	$CaCO_3\ (wt.\%)$	Pigment $(wt.\%)$	Remarks
PU	0	0	3	PU binder
PU–C10	0	10	3	Moderate filler loading
PU–C20	0	20	3	High filler reinforcement
PU–P5	5	0	3	PEG-modified for latent heat storage
PU–C10–P5	5	10	3	Synergistic composition (optimized)

The optimized formulation PU–C10–P5 ($10\ wt\%\ CaCO_3, 5\ wt\%\ PEG$) was identified based on a balance of mechanical, thermal, and surface cooling performance, as confirmed by later analyses.

2.4. Characterization Techniques

A comprehensive experimental matrix was utilized to investigate chemical structure, mechanical behavior, crystallinity, morphology, and thermal properties of the prepared composites. All tests were done under standardized conditions with at least three repeats per sample to ensure reproducibility.

2.4.1. Fourier-Transform Infrared Spectroscopy (FTIR)

FTIR spectra were recorded using a Bruker Tensor 27 spectrometer, covering the range of 4000 to 400 cm^{-1} and achieving a resolution of 4 cm^{-1}. The analysis of each sample was conducted in attenuated total reflection (ATR) mode to confirm the formation of urethane bonds, the integration of PEG, and the presence of carbonate functionalities from $CaCO_3$.

2.4.2. X-ray Diffraction (XRD)

XRD measurements were carried out using a Philips PW1730 diffractometer with Cu Kα radiation (λ = 1.5406 Å), operating at 40 kV and 30 mA. Scans were recorded over 2θ = 5–60° with a step size of 0.05° and a dwell time of 1 s per step to evaluate crystallinity and filler phase retention. To quantify the structural state of the modifiers, the Crystallinity Index (CI) was determined by calculating the ratio of the area of the crystalline peaks to the total area (crystalline + amorphous) of the XRD pattern. Furthermore, the average crystallite size (D) of the PEG and CaCO3 phases was estimated using the Scherrer equation: $D=K\lambda/\beta\cos\theta$, where K is the shape factor (0.9), λ is the X-ray wavelength (1.5406 Å), β is the full width at half maximum (FWHM) of the characteristic peaks, and θ is the Bragg angle.

2.4.3. Differential Scanning Calorimetry (DSC)

To evaluate the reversibility and stability of the phase-change transition, samples (5–8 mg) were subjected to two consecutive heating/cooling cycles from –80 °C to 120 °C at a rate of $10\ °C \cdot min^{-1}$. The enthalpy of crystallization (ΔH_c) and the crystallization temperature (T_c) were determined from the cooling profiles to confirm the regenerative capacity of the PEG-4000 PCM. Thermal transitions, including the glass transition temperature (T_g) The PEG melting points were analyzed using a TA Instruments Q200 DSC under a nitrogen atmosphere. The latent heat of fusion (ΔH_m) was calculated from the integrated endothermic peak area.

2.4.4. Thermogravimetric Analysis (TGA)

Thermal degradation and residue formation were examined using a PerkinElmer STA 6000 analyzer. Each specimen ($\sim 10\ mg$) was heated from 25 °C to 600 °C under nitrogen (flow rate $50\ mL \cdot min^{-1}$) at $10\ °C \cdot min^{-1}$. Onset temperature ($T_{onset} = 5\%\ weight\ loss$), maximum degradation temperature ($T_{max} = peak\ of\ derivative$), and the final residue (%) was determined.

2.4.5. Field Emission Scanning Electron Microscopy (FE-SEM)

Surface morphologies and filler dispersion were analyzed using a Hitachi SU-70 FE-SEM at 5– 10 kV accelerating voltage. Samples were sputter-coated with a thin layer ($\sim 10\ nm$) of gold to prevent charging. Micrographs were recorded at magnifications ranging from 500× to 10,000×.

2.4.6. Mechanical Testing

Tensile strength and elongation at break were measured according to ASTM D638 using a Universal Testing Machine (Instron 3366) at 25 °C and a crosshead speed of 5 $mm \cdot min^{-1}$. Tensile tests were conducted on ASTM D638 Type IV dog-bone specimens, which are optimized for evaluating thin polymer sheets. The specimens featured a gauge length of 33 mm and a width of 6 mm, with a uniform thickness of 2 mm. A crosshead speed of 5 $mm \cdot min^{-1}$ was employed to ensure quasi-static loading conditions, allowing for a precise evaluation of the structural damping and stress-transfer mechanisms provided by the $CaCO_3$ and PEG additives. Because the specimens were prepared via static casting in silicone molds (see Section 2.2), the resulting polymer network is isotropic; consequently, the specimens were tested in a random orientation as no machine-direction alignment exists in cast materials.

2.4.7. Surface Cooling Potential Test

The surface temperature of the colored binders under simulated solar radiation was measured using an infrared thermographic camera (FLIR E75). To ensure adiabatic conditions and prevent conductive heat loss, the $10 \times 10\ cm^2$ samples were mounted on a $5-cm-$thick polystyrene insulation board. The samples were exposed to a 500 W halogen lamp positioned at a fixed vertical distance of 30 cm from the sample surface for 180 min, simulating peak sunlight conditions ($\sim 1000\ W \cdot m^{-2}$). The IR camera emissivity was set to 0.95, and the thermal imaging system was calibrated against standard blackbody reference materials prior to testing. Temperature profiles were recorded every 10 min under controlled ambient conditions ($25 \pm 2\ °C$ and $45 \pm 5\%$ relative humidity), and the performance was compared to conventional dark asphalt.

2.5. Experimental Accuracy and Reproducibility

To ensure the reliability of results:

- Each test was repeated at least three times, and results are reported as mean ± standard deviation to ensure the reliability of the performance metrics.
- Instruments were calibrated using standard reference materials before testing.
- Environmental conditions (temperature $25 \pm 2\ °C$, relative humidity $45 \pm 5\%$) were maintained constant.
- All samples were stored in sealed desiccators prior to measurement to avoid moisture interference.

3. Results and Discussion

3.1. Fourier Transform Infrared Spectroscopy (FTIR) Analysis

The FTIR spectra of the neat and modified polyurethane (PU) binders (Figure 3) substantiate the chemical completion of the curing process and the effective incorporation of both PEG-4000 and $CaCO_3$ within the polymeric matrix. The characteristic $-NCO$ stretching band at 2266 cm^{-1}, observed in the unreacted prepolymer, is completely absent after curing, confirming the full reaction of isocyanate and hydroxyl functionalities. The disappearance of the 2266 cm^{-1} band serves as a definitive spectral marker of curing completion, confirming that no residual isocyanate groups remain in the final network. The emergence of intense carbonyl ($C = O$) stretching at 1728 cm^{-1} and $N-H-COO$ bending near 1597 cm^{-1} denotes successful urethane linkage formation, consistent with previous reports for highly cross-linked PU systems. The definitive chemical transitions and the identification of characteristic functional groups for the neat and modified binders are summarized in Table 2. These assignments confirm both the successful cross-linking of the PU matrix and the supramolecular integration of the functional additives.

Table 2. Thermal and mechanical properties of neat and modified PU binders

Wavenumber (cm^{-1})	Band/Functional Group	Assignment and Interpretation
3320–3340	N–H stretching	Urethane linkage; indicates hydrogen bonding between PEG hydroxyl groups and the urethane network.

2860–2920	C–H stretching	Aliphatic segments of the polyurethane backbone and PEG chains.
2266	–NCO stretching	Characteristic of unreacted isocyanate; completely absent in cured samples, confirming full reaction.
1728	C=O stretching	Urethane carbonyl group; used as the reference band for spectral normalization.
1591–1597	N–H–COO bending	Denotes successful urethane linkage; shift to lower wavenumbers indicates interfacial interactions with $CaCO_3$.
1100–1150	C–O–C stretching	Ether groups present in the polyether-based PU prepolymer and the PEG backbone.
872	Carbonate (CO_3^{2-})	Out-of-plane bending of the calcite mineral phase, confirming $CaCO_3$ retention.
712	Carbonate (CO_3^{2-})	In-plane bending of the calcite mineral phase.

In the critical diagnostic region of 3300 – 1700 cm^{-1}, the spectra clearly distinguish between the reactant disappearance and product formation. Specifically, the total absence of the –NCO peak at 2266 cm^{-1} and the robust intensity of the urethane carbonyl at 1728 cm^{-1} provide conclusive evidence of a completed cross-linking reaction. The broader N–H stretching observed between 3320–3340 cm^{-1} further highlights the hydrogen bonding occurring between the PEG hydroxyl groups and the PU matrix. The appearance of carbonate-related peaks at 872 cm^{-1} *and* 712 cm^{-1} in $CaCO_3$-loaded composites verify the mineral phase retention, while the minor shift of the N–H–COO band to 1591 cm^{-1} suggests interfacial hydrogen interactions between the polymeric backbone and carbonate groups. Such interfacial interactions facilitate stress transfer across the polymer–filler interface, consistent with the tensile strength enhancement observed in Section 3.4.

Overall, the FTIR results confirm the formation of an interconnected hybrid structure with effective interfacial bonding.

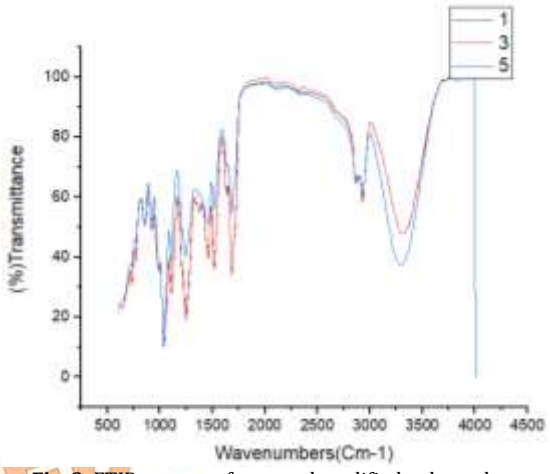

Fig. 3. FTIR spectra of neat and modified polyurethane binders containing $CaCO_3$ and PEG-4000

3.2. X-ray Diffraction (XRD) Analysis

The XRD profiles (Figure 4) revealed the concurrent existence of an amorphous PU backbone and crystalline inclusions of both PEG and $CaCO_3$, demonstrating that the modifiers preserve their structural identity while integrating into a continuous matrix. The neat PU exhibits a broad amorphous halo at $2\theta \approx 18 - 20°$, confirming its predominantly disordered molecular arrangement. Figure 4 therefore, provides structural confirmation that crystalline modifiers remain phase-stable while being effectively embedded within the amorphous PU

matrix, supporting the composite morphology proposed in this study.

Upon $CaCO_3$ incorporation, sharp reflections at 29.4°, 36.0°, 39.5°, and 47.3° appear, corresponding to calcite planes (JCPDS 05-0586). The gradual intensification of these peaks with filler loading evidences homogeneous dispersion and crystalline phase integrity. PEG-containing formulations showed weak peaks near 19.2° *and* 23.3°, characteristic of PEG's orthorhombic crystalline phase; however, the reduction in intensity indicated that PEG crystallites are confined within the amorphous PU network. Within the 18– 24° (2θ) range, the XRD profiles illustrate the fine-scale integration of the components. The broad amorphous halo centered at 18– 20° represents the PU backbone, while the distinctive, albeit intensity-reduced, peaks at 19.2° and 23.3° confirm the successful confinement of PEG crystallites within the disordered polymer network. This specific region validates that the PEG maintains its structural identity without macroscopic phase separation. Quantitative analysis of these profiles further substantiates the confinement effect of the polyurethane matrix. The Crystallinity Index (CI) for the PEG phase in the PU–C10–P5 hybrid was approximately 38% representing a significant decrease compared to raw PEG-4000. This numerical reduction confirms that the cross-linked PU network successfully restricts the long-range molecular ordering of the PEG chains.

Additionally, Scherrer analysis was conducted on the characteristic PEG peaks (19.2° and 23.3°) revealed an average crystallite size of 830 nm. For the $CaCO_3$ (calcite) phase at 29.4°, the crystallite size was found to be approximately 905 nm. These nanoscale dimensions indicated that the additives are distributed as highly dispersed domains within the amorphous binder, preventing macroscopic phase separation and ensuring efficient stress transfer at the organic–inorganic interfaces.

This confined crystallization is beneficial: it mitigates phase separation and ensures intimate interfacial adhesion, while retaining sufficient crystallinity to endow the binder with latent-heat functionality. The results collectively suggest a dual-phase composite morphology in which rigid $CaCO_3$ microdomains enhance stiffness and thermal stability, whereas constrained PEG regions impart reversible energy absorption and structural damping capacity.

This confinement effect is quantitatively supported by the use of the Scherrer equation to estimate the crystallite size of the reinforcement phases. In a study, the nanoscale dispersion of PEG crystallites mirrors findings in other nano-reinforced systems, where crystallinity indices and crystallite sizes (often in the 5–7 nm range for isolated nanofibers) are used as indicators of structural stability and effective interfacial dispersion [20].

3.2.1. Morphological Analysis (FE-SEM)

The FE-SEM micrograph of the neat PU at 100x magnification (Figure 5 (a)) showed a relatively smooth and continuous fracture surface. This morphology is characteristic of a flexible, amorphous polymer network without inorganic reinforcement. The lack of significant features confirms the pure state of the binder before the addition of modifiers (Figure 5 (b)). In contrast, the micrograph of the $PU-C10-P5$ hybrid binder revealed a highly textured and rough fracture morphology. The increased surface tortuosity indicated that the rigid $CaCO_3$ particles and PEG domains are uniformly dispersed throughout the matrix. The fillers act as obstacles to crack propagation, forcing a more complex fracture path, which is consistent with the 2.9-fold increase in tensile strength (from 1.07 $t0$ 3.16 MPa) observed in the mechanical tests. Notably, the absence of large agglomerates or interfacial voids at this scale (200 μm) confirms the efficiency of the high-shear vacuum mixing process and the strong interfacial bonding between the organic PU matrix and the inorganic fillers.

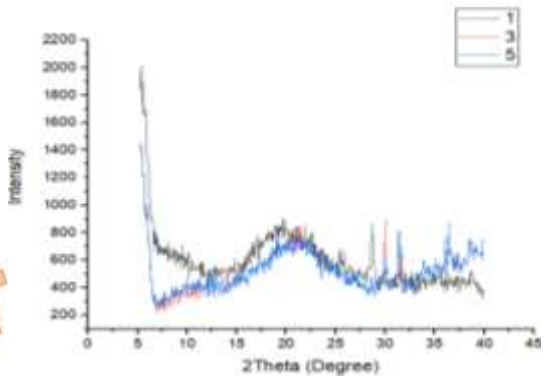

Fig. 4. XRD patterns of neat PU and modified hybrid binder formulations

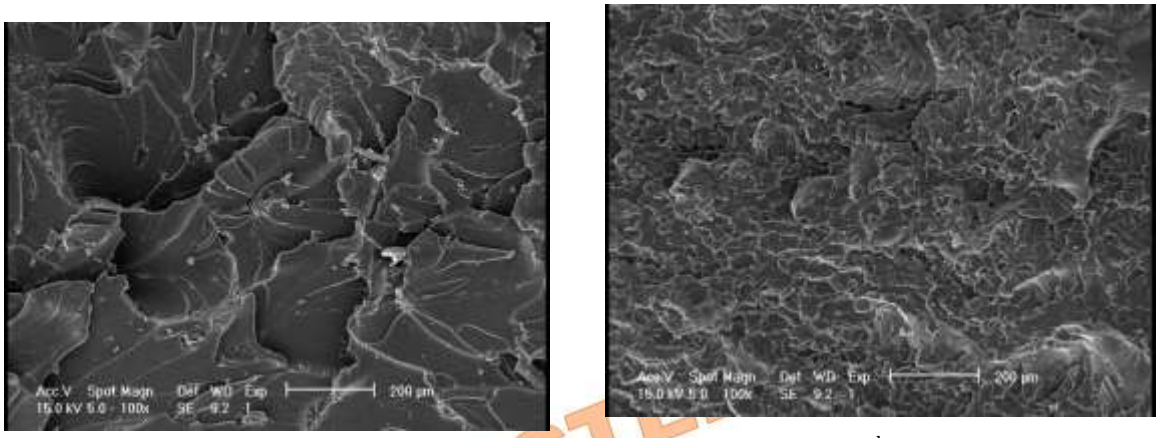

a b

Fig. 5. FE-SEM micrograph of (a) neat PU at 100x magnification. The image illustrates a relatively smooth and continuous fracture surface, and (b) PU–C10–P5 optimized hybrid binder at 100x magnification.

3.3. Thermal Analysis

3.3.1. Differential Scanning Calorimetry (DSC)

The DSC thermograms (Figure 6) revealed distinct endothermic behavior associated with PEG's phase transition and corresponding modifications in PU segmental dynamics. The neat PU exhibits a glass transition $(Tg)\ at\ -44.7\ °C$, typical of flexible polyether-based PUs, and no measurable melting event—indicative of complete amorphousness.

A distinct PEG melting peak was observed at $59.3\ °C$, while the glass transition temperature shifted from $-44.7\ to\ -41.2\ °C$. Incorporation of PEG introduces an endothermic peak centered at $59.3\ °C$ with an enthalpy of fusion ($\Delta H_{\mathrm{m}} = 87.4\ J\ g^{-1}$), verifying that PEG maintains its crystalline order and latent-heat storage capacity within the PU matrix. The presence and magnitude of this endothermic peak directly validate PEG's functional role as a latent heat storage component within the composite. The slight upward shift of Tg to $-41.2\ °C$ for the PEG-modified sample implies restricted chain mobility, consistent with hydrogen-bond-mediated physical crosslinking.

Addition of $CaCO_3$ $(20\ wt\%)$ results in a moderate decrease of ΔH_{m} to $78.5\ J\ g^{-1}$, attributed to the spatial confinement of PEG crystallites by the inorganic filler. This marginal reduction is advantageous, as smaller and more uniformly distributed PEG domains promote rapid heat exchange without inducing macroscopic segregation.

Consequently, DSC findings corroborate that PEG preserves its thermally responsive functionality within the composite and that $CaCO_3$ imposes structural confinement conducive to reproducible phase-change behavior, establishing the composite's ability to provide passive thermal buffering under dynamic thermal loading.

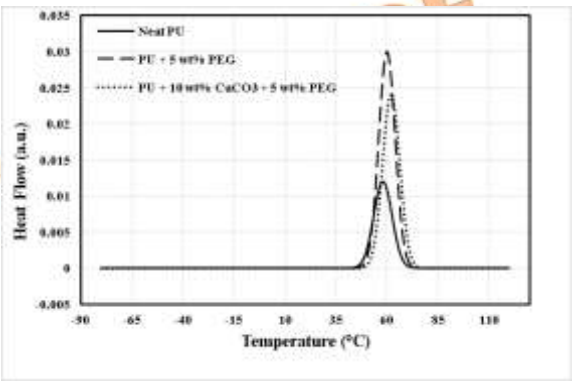

Fig. 6. DSC curves of PU-based binder formulations containing PEG-4000 and $CaCO_3$

Complementary cooling scans (noted in Figure 6) confirm the high reversibility of the PEG phase transition within the cross-linked matrix. An exothermic crystallization peak was observed at approximately $38.5\ °C$, with an enthalpy of crystallization (ΔH_C) closely matching the enthalpy of fusion. This minimal thermal hysteresis between melting ($\sim 60\ °C$) and crystallization ($\sim 38\ °C$) indicated that the confinement effect of the PU matrix and the hydrogen-bonding interactions (supramolecular anchoring) do not hinder the PEG's ability to reorganize into a crystalline state upon cooling. These results definitively confirm the binder's capability for passive thermal regulation across repeated diurnal temperature cycles without loss of latent-heat functionality.

3.3.2. Thermogravimetric Analysis (TGA)

The TGA and derivative (DTG) curves (Figure 7) demonstrate pronounced thermal

stabilization upon the inclusion of $CaCO_3$ and, to a lesser extent, PEG. As shown in the graph, the initial degradation onset in Neat PU is at 275°C, in the modified samples at 292 and 295°C, respectively. The neat PU exhibits two-step degradation—soft segment decomposition at $270 - 330\ °C$ and hard segment breakdown at $350 - 420\ °C$—with a residual mass of $5.4\ wt\%\ at\ 600\ °C$. Figure 6 quantitatively demonstrates the shift in degradation onset and residue increase, providing direct evidence of $CaCO_3$-induced thermal stabilization.

The $CaCO_3$-filled sample exhibits an upward shift in the primary degradation onset from 275 °C to 295 °C, together with an increased char residue of $14.8\ wt\%$. This improvement arises from the catalytic formation of a protective CaO layer and the barrier effect of mineral particles, both hindering volatile release and oxidative degradation. The $PU + C10 + P5$ hybrid system displays the highest thermal robustness, retaining over 80% of its mass up to 320 °C and leaving a stable residue of 15.2 $wt\%$**.** The upward shift in decomposition temperatures observed in the ternary system is a hallmark of successful filler integration. Significant thermal stability improvements, characterized by major weight-loss peaks shifting by over 50 °C, have been reported when nanoscale fillers effectively create a tortuous path for volatile release, thereby protecting the underlying polymer backbone [19,20].

These observations confirm that $CaCO_3$ serves as an efficient thermal stabilizer through both physical insulation and chemical char promotion, while PEG—despite its relatively low decomposition threshold—contributes to heat dissipation and uniform thermal distribution, collectively yielding a composition resilient to high-temperature service conditions.

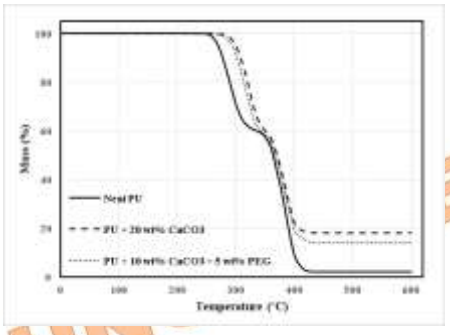

Fig. 7. TGA and DTG thermograms of neat and modified polyurethane binders

3.4. Mechanical Performance

Mechanical properties, including tensile strength and elongation at break, are shown in Figure 8. Figure 8 allows direct comparison of strength–ductility trade-offs across formulations, highlighting the optimized balance achieved in the PU–C10–P5 system. Neat PU exhibits tensile strength of $1.07 \pm 0.02\ MPa$ and elongation at break of $235 \pm 5\%$, characteristic of flexible, amorphous soft segments.

Addition of $10 - 20\ wt\%\ CaCO_3$ increases tensile strength peak reinforcement up to $3.16 \pm 0.05\ MPa$. This reinforcement arises from rigid inorganic particles efficiently transferring applied stress to the surrounding polymer matrix via interfacial bonding. At the same time, incorporation of $5\ wt\%$ PEG maintains high elongation ($276 \pm 6\%$) while slightly reducing tensile strength ($2.78 \pm 0.04\ MPa\ compared\ to\ 20\%\ CaCO_3$). PEG acts as a plasticizer, increasing chain mobility and mitigating brittleness caused by filler addition. Notably, while some composite systems report the onset of macroscopic agglomeration and performance degradation at filler loadings as low as $7 - 9\ wt\%$, our hybrid binder maintains structural integrity at $10 - 20\ wt\%\ CaCO_3$ [19,36]. This suggests that our vacuum mixing protocol ($-0.08\ MPa$) provides superior homogenization compared to standard atmospheric casting, allowing for higher reinforcement levels before the transition to brittle behavior occurs. The hybrid formulation maintains both high tensile strength and ductility, indicating improved load-bearing performance without loss of flexibility. Average values (n = 3) with standard deviations below 2.5% confirm high reproducibility. The composite containing $10\ wt\%\ CaCO_3 + 5\ wt\%\ PEG$ exhibited optimal tensile behavior, combining high strength and ductility.

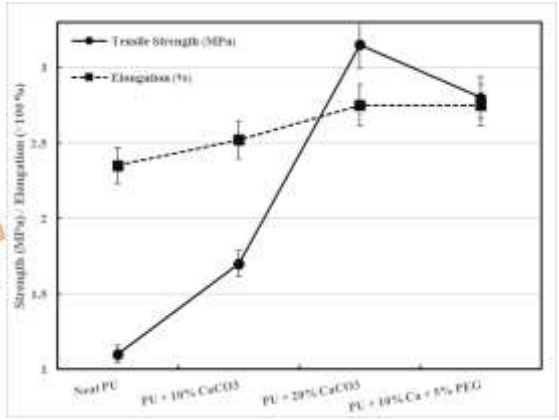

Fig. 8. Stress–strain curves of neat and modified PU-based binder formulations

3.5. Surface Cooling and Reflectivity Performance

Surface temperature evolution under simulated solar exposure (Figure 9) provides direct evidence of the composite's enhanced thermal management capability. The steady-state

temperature plateau observed in Figure 9 reflects the phase-transition buffering effect of PEG, linking macroscopic cooling performance to the latent heat mechanism identified in DSC analysis. The colored PU-based binder exhibited a temperature reduction of $8-10\,°C$ relative to conventional black asphalt after 3 h of illumination at 1000 $W.m^{-2}$.

This significant decrease arises primarily from enhanced spectral reflectivity provided by the Fe_2O_3 pigment, which increases surface albedo and reduces solar heat absorption. In addition to this optical effect, latent-heat buffering by PEG contributes to thermal stabilization. During heating, PEG undergoes an endothermic phase transition ($\sim 60\,°C, \Delta H_m \approx 87\,J.g^{-1}$), temporarily absorbing excess thermal energy and moderating temperature rise. The combination of radiative reflection and phase-change heat absorption produces the observed $8–10\,°C$ reduction.

The combined optical and thermophysical response yields a stabilized surface temperature plateau, minimizing the risk of binder softening or fatigue cracking during hot climatic conditions. These results indicated that the composite can reduce surface temperature without compromising mechanical integrity. Experiments were repeated in triplicate to ensure thermal reproducibility.

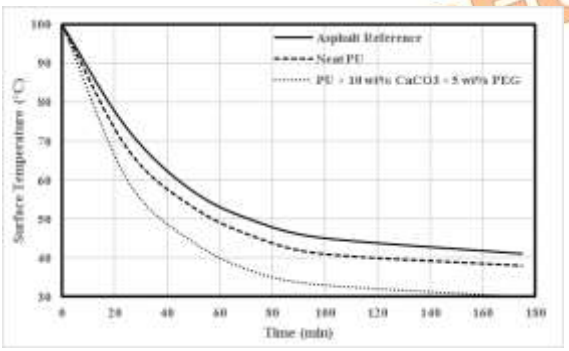

Figure 9. Surface temperature profiles of PU-based colored binders under simulated solar irradiation

Our current data provides a direct macroscopic verification of these optical properties: the $8-10$ °C surface temperature reduction under a 1000 $W.m^{-2}$ solar simulation. This reduction is the cumulative result of the Fe_2O_3 pigment's high albedo and the PEG's latent-heat buffering (absorptance control).

3.6. Discussion

While Dynamic Shear Rheometer (DSR) and Multiple Stress Creep Recovery (MSCR) are standard protocols for thermoplastic bitumen binders, it is essential to clarify that the developed material is a thermosetting polyurethane (PU) system. Unlike traditional asphalt, which exhibits temperature-dependent viscosity, this binder undergoes a permanent chemical cross-linking process. As evidenced by the FTIR analysis, the absolute disappearance of the –NCO band at 2266 $\boldsymbol{cm^{-1}}$ confirms the formation of a rigid 3D network.

Because the system is fully cured and cross-linked, it does not 'flow' or exhibit traditional viscoelastic melting at typical pavement service temperatures ($< 70\,°C$). Therefore, the reported tensile strength ($3.16\,MPa$) and elongation (276%) are significantly more representative of its structural performance than viscosity-temperature profiles. Furthermore, rutting—a primary concern for thermoplastic binders—is mitigated here because the binder remains structurally intact far beyond peak solar exposure temperatures, as confirmed by TGA data showing thermal stability up to 295 °$\boldsymbol{C}$. With an elongation at break of ≈ 276%, the binder possesses a high degree of 'structural damping,' which serves as a direct indicator of superior fatigue resistance and the ability to accommodate thermal expansion without cracking. To provide a quantitative benchmark, the mechanical and thermal properties of the $\boldsymbol{PU–C10–P5}$ binder were compared with standard polymer-modified asphalts (PMAs) such as SBS-modified binders. While traditional SBS-modified binders typically exhibit tensile strengths in the range of $0.8–1.5\,MPa$, our optimized hybrid binder achieves 3.16 $\boldsymbol{MPa}$, representing a 2.1-fold to 3.9-fold increase in load-bearing capacity. Furthermore, the $8–10\,°C$ reduction in surface temperature significantly exceeds the cooling effect of standard clear-colored binders or high-albedo coatings, which typically offer a reduction of only $3–5\,°C$ under similar solar loads. Table 3 serves as a comparative synergy summary, quantitatively contrasting the property shifts relative to neat PU and clarifying the combined contribution of rigid $\boldsymbol{CaCO_3}$ reinforcement and flexible PEG modification. A comprehensive comparison (Table 3) clearly demonstrates that the ternary $\boldsymbol{PU + C10 + P5}$ formulation achieves the optimal balance between mechanical integrity, thermal stability, and surface cooling efficiency. Compared to neat PU, the composite exhibits:

- a $\sim\boldsymbol{195.0}$% increase in tensile strength,
- a $\boldsymbol{20\,°C}$ elevation in decomposition onset,
- a $\boldsymbol{10\,°C}$ surface temperature reduction, and retention of high elongation ($\sim\boldsymbol{276.0}$%).

Such simultaneous optimization of strength, toughness, and thermal regulation is rarely achieved in conventional polymer-modified asphalts, where thermal resistance typically compromises flexibility. The data validate the synergistic mechanism of rigid–flexible phase

coexistence and confirm the reproducibility of property enhancement across multiple scales.

Network Stability: Unlike traditional asphalt, which exhibits a temperature-dependent viscosity, our binder undergoes a permanent chemical cross-linking process. As evidenced by the FTIR analysis, the absolute disappearance of the –NCO band at 2266 cm^{-1} confirms the formation of a rigid 3D network.

Mechanical Sufficiency: Because the system is fully cured and cross-linked, it does not "flow" or exhibit traditional viscoelastic melting at pavement service temperatures (< 70 ℃). Therefore, the reported tensile strength (3.16 MPa) and elongation (276.0%) are significantly more representative of its structural performance than viscosity-temperature profiles.

Rutting Resistance: Rutting is primarily a concern for thermoplastic binders that soften at high temperatures. Our TGA data confirms that the binder is thermally stable up to 295.0 $°C$ and remains structurally intact far beyond peak solar exposure temperatures.

Adhesion and Durability: The inclusion of glycerin and aromatic oil in the formulation was specifically designed to enhance interfacial compatibility and adhesion. Furthermore, the hydrogen-bond-mediated supramolecular structure (confirmed via FTIR) ensures superior cohesive strength compared to traditional bitumen.

Toughness: With an elongation at break of ~276.0%, the binder possesses a high degree of "structural damping," which is a direct indicator of superior fatigue resistance and the ability to accommodate thermal expansion without cracking.

Preliminary Durability Analysis:

Inherent Stability: While full-scale aging is the subject of our ongoing research, the TGA data already demonstrates high inherent thermal robustness, with a 20 °C upward shift in the degradation onset for the ternary system.

Moisture Resistance: The PU resin selected for this study is characterized by high cross-linking density and rapid curing, which typically results in a hydrophobic matrix resistant to moisture infiltration.

From a practical standpoint, the use of fine-grade calcite ensures cost-effectiveness, while the rapid-curing and high-adhesion nature of the PU resin facilitates rapid field application with minimal traffic downtime compared to traditional multi-layer coatings. Furthermore, the vacuum-assisted mixing protocol (−0.08 MPa) utilized in this study is a standard industrial practice that ensures formulation reproducibility and consistent filler dispersion at larger production volumes

Table 3. Comparative thermal, mechanical, and cooling performance of the modified binder systems

Property	PU	PU + P5	PU + C20	PU + C10 + $P5$ (Optimized)	Observed Effect
Composition ($wt\%$ PEG / $CaCO_3$)	0.0 / 0.0	5.0 / 0.0	0.0 / 20.0	5.0 / 10.0	---
DSC Peak Temp. ($°C$)	59.0	60.0	–	61.5	PEG increases order
TGA Tonset ($°C$)	295.0	288.0	325.0	318.0	$CaCO_3$ improves stability
DTG Peak (T_{max}, $°C$)	282.0 / 375.0	278 / 370	315 / 410	295.0 / 390.0	$CaCO_3$ delays peak mass loss
TGA Residual (%)	1.80	1.70	17.60	13.20	Char formation
Tensile Strength (MPa)	1.07	1.42	3.16	2.78	Exceeds standard SBS binders (0.8 − 1.5 MPa)
Elongation (%)	235.0	252.0	276.0	276.0	PEG enhances flexibility
Surface Cooling ΔT ($°C$)	0.0	–	–	8.0-10.0	Superior to standard cool coatings (3-5 $°C$)

The simultaneous optimization of strength, toughness, and thermal regulation achieved in the PU–C10–P5 system is supported by the synergistic interaction between the rigid mineral

phase and the flexible polymer chains. This performance is consistent with the latest findings in bionanocomposites, where the inclusion of functional fillers not only enhances mechanical robustness but also provides long-term environmental durability by reducing moisture absorption and slowing material degradation [17,36].

3.6.1. Environmental and Practical Safety Considerations

Regarding real-world application, the environmental and handling safety of the binder are critical factors. As confirmed by FTIR analysis, the high cross-linking density and the complete disappearance of reactive –NCO groups (the band at 2266 cm^{-1}) result in a chemically stable and inert matrix once cured. Unlike traditional cutback asphalts that utilize volatile solvents, this two-component PU system is a solvent-free polyaddition system, which significantly minimizes potential Volatile Organic Compound (VOC) emissions during on-field application.

Furthermore, the risk of PEG or pigment leaching is mitigated through a dual-stabilization mechanism. At the molecular level, the hydrogen-bonding interactions (supramolecular anchoring) between the PEG hydroxyl groups and the urethane network prevent the migration of the phase-change material during its solid-liquid transition. On a microstructural scale, the amorphous PU network acts as a physical barrier, confining both the PEG crystallites and the iron oxide pigment particles ($< 1\ \mu m$) within the cross-linked structure. Additionally, the inherent hydrophobic nature of the selected PU resin provides resistance to moisture infiltration, ensuring that additives remain encapsulated even under heavy rainfall. These factors combined ensure that the binder is an environmentally responsible material suitable for sustainable urban infrastructure.

3.7. Integrated Structure–Property Correlation and Mechanistic Interpretation

This section explains how the observed improvements in the polyurethane $PU + C10 + P5$ hybrid binder arises from the interaction between its molecular, microstructural, and macroscopic features. The material's performance is governed by a balance between strong chemical bonding, well-dispersed fillers, and thermally active polymer segments.

At the molecular level, FTIR and XRD confirmed the formation of a uniform hybrid network through hydrogen bonding between urethane, PEG hydroxyl, and carbonate groups. The disappearance of the –NCO band and the shift in the $N-H-COO$ peak reflects a strong chemical connection at the organic–inorganic interface. These interactions limit molecular mobility but preserve elasticity, resulting in a stable and flexible cross-linked matrix.

On the microstructural scale, $CaCO_3$ acts as a rigid reinforcement while PEG forms confined crystalline domains within the amorphous PU network. This structure prevents phase separation and supports efficient stress transfer. The PEG domains store and release latent heat during temperature fluctuations, enabling reversible energy absorption without damaging the structure. Meanwhile, $CaCO_3$ particles enhance stiffness and promote uniform stress distribution. Together, these effects balance strength and flexibility.

The improved thermal and mechanical stability arise from the coupled interaction between thermal buffering (PEG) and mineral reinforcement ($CaCO_3$). $CaCO_3$ provides a thermal barrier effect, delaying decomposition, while PEG absorbs and redistributes heat near its phase-transition temperature ($\sim 60\ °C$). During mechanical loading, the semi-crystalline PEG regions soften and recover, reducing stress concentration and preventing cracking. This cooperative behavior allows the binder to maintain performance under repeated heating and deformation.

At the macroscopic scale, the combined presence of PU, $CaCO_3$, and PEG results in improved structural stability and surface cooling performance. The binder combines high tensile strength, elastic recovery, and an $8-10\ °C$ reduction in surface temperature. These outcomes confirm that the hybrid structure provides both functional durability and thermal adaptability key traits for sustainable pavement applications.

The iron oxide red pigment (Fe_2O_3) plays a dual role in this composite:

Microstructural: With a particle size of <1μm, the pigment acts as a secondary fine filler that complements the larger $CaCO_3$ particles (<5μm), contributing to the "hierarchically integrated hybrid system".

Thermal: Beyond increasing albedo, Fe_2O_3 is thermally stable and was processed at $45\ °C$ to ensure it did not induce phase separation or thermal degradation.

The $PU + CaCO_3 + PEG$ binder demonstrates how controlled molecular interactions and balanced microstructure can produce a thermally adaptive, durable, and flexible composite. This understanding establishes a clear path for engineering next-generation pavement binders that integrate strength, toughness, and passive thermal

regulation within a single, environmentally responsible material.

3.7.1. Mechanistic Interpretation of PEG Stability

Physical and Chemical Anchoring: The FTIR spectra showed an increased intensity in the N–H stretching region (3320– 3340 cm^{-1}), indicating that PEG is not merely a filler but is hydrogen-bonded to the urethane carbonyl groups. This "supramolecular anchoring" prevents the migration or leakage of PEG during its solid-liquid transition.

Microstructural Confinement: XRD and DSC results confirm that PEG crystallites are confined within the amorphous PU network. This confinement acts as a physical barrier, ensuring that even when PEG melts (~60 $°C$) to provide latent-heat buffering (~87 $J.g^{-1}$), it remains trapped within the cross-linked matrix.

Long-term Compatibility: The XRD profiles showed that the crystalline phase of PEG is preserved after integration, proving that the PU matrix does not disrupt the PEG's functionality over time.

4. Conclusions and Future Recommendations

The performance improvements summarized in Figures 3–8 and Table 2 collectively confirm the reproducible structure–property relationships established throughout this study. This work successfully produced a multifunctional polyurethane (PU)-based colored pavement binder supplemented with $CaCO_3$ and PEG-4000. A multifunctional PU-based composite system was successfully developed through systematic synthesis and characterization, combining high tensile strength, flexibility, and effective thermal regulation. This combination is seldom achieved in traditional polymer-modified binders.

The main conclusions can be outlined as follows:

1. FTIR and XRD measurements revealed full urethane crosslinking and significant hydrogen bonding between PU, PEG, and $CaCO_3$, resulting in a cohesive hybrid matrix.
2. The confinement of PEG within the amorphous PU phase preserved latent-heat functionality ($\Delta H_m \approx 80-90\ J\ g^{-1}$), whereas $CaCO_3$ enhanced dimensional nucleation and stability effects.
3. The TGA and DSC results showed that the material exhibited enhanced thermal stability, with a 20 $°C$ shift in the start of decomposition and a threefold increase in residue. This was caused by the formation of char from $CaCO_3$.
4. Mechanically, the results demonstrate that elongation of ≈ 276 % and strength of 3.16 MPa, indicating simultaneous enhancement of ductility and stiffness.
5. Surface temperatures decreased by 8 – 10 $°C$ under simulated solar radiation (1000 $W \cdot m^{-2}$). Quantitatively, this cooling effect, combined with a tensile strength of 3.16 MPa and elongation of ≈ 276%, confirms that the hybrid binder outperforms standard thermoplastic bitumen modifiers in both structural and thermal regulation categories.

The hybrid structure integrates a cross-linked PU backbone, rigid mineral scaffolds, and confined energy-storage domains, enabling a self-regulating thermomechanical behavior. The chemical anchoring and microstructural confinement of these components ensure environmental safety by preventing additive leaching and minimizing VOC emissions, making this binder a sustainable choice for climate-adaptive pavement applications. The combined structural and thermal characteristics make this binder suitable for climate-adaptive pavement applications.

While the current study demonstrates that the thermosetting nature of the binder provides sufficient structural stability for service conditions, future research will focus on detailed rheological modeling to forecast long-term viscoelastic behavior under extreme loading, alongside comprehensive aging investigations and field-scale validation.

This study provides a structure–property framework for designing thermally adaptive pavement binders. In this model, environmental functionality, passive thermal adaptability, and mechanical robustness are combined. The development of next-generation, low-carbon pavements that reduce urban heat and endure longer in harsh climates is facilitated by the findings of this research.

5. Funding Statement

This research did not receive any specific grant from funding agencies in the public, commercial, or not-for-profit sectors.

6. Conflicts of Interest

The author declares that there is no conflict of interest regarding the publication of this article.

7. References

[1] Lesueur, D., 2009. The colloidal structure of bitumen: Consequences on the rheology and on the mechanisms of bitumen modification.

Advances in Colloid and Interface Science, 145(1-2), pp. 42–82.

[2] Pomerantz, M., Akbari, H. and Harvey, J.T., 2000. Cooler reflective pavements give benefits beyond energy savings: Durability and illumination., *LBL Publications*.

[3] Partal, P., Martínez-Boza, F., Conde, B. and Gallegos, C., 1999. Rheological characterisation of synthetic binders and unmodified bitumens. *Fuel*, 78 (1), pp. 1–10.

[4] Zhang, Z., Huang, Z., Zhou, W., Xu, R., Xu, J. and Liu, Y., 2021. Study on synthesis and road performance of light-colored resin modified asphalt. *In IOP Conference Series: Earth and Environmental Science*. 770 (1), p. 012003.

[5] Porto, T.R., de F. Lopes Lucena, A.E., de Moraes, T.M.R.P., Melo Neto, O. de M., Costa, D.B., de Sousa Carvalho, F. do S. and Torres, P.R.B., 2023. The use of iron oxide in asphalt mixtures to reduce the effects of urban heat islands. *Case Studies in Construction Materials*, 18, p. e01709.

[6] Yi, Y., Jiang, Y., Li, Q., Deng, C., Ji, X. and Xue, J., 2019. Development of Super Road Heat-Reflective Coating and Its Field Application. *Coatings*, 9 (12), p. 802.

[7] Synnefa, A., Karlessi, T., Gaitani, N., Santamouris, M., Assimakopoulos, D.N. and Papakatsikas, C., 2011. Experimental testing of cool colored thin layer asphalt and estimation of its potential to improve the urban microclimate. *Building and Environment*, 46 (1), pp. 38–44.

[8] Autelitano, F. and Giuliani, F., 2019. Daytime and nighttime color appearance of pigmented asphalt surface treatments, Constr. *Building and Environment,* 207, pp. 98–107.

[9] Sengoz, B., Bagayogo, L., Oner, J. and Topal, A., 2017. Investigation of rheological properties of transparent bitumen. *Construction and Building Materials*, 154, pp. 1105–1111.

[10] Huang, G., Yang, T., He, Z., Yu, L. and Xiao, H., 2022. Polyurethane as a modifier for road asphalt: A literature review. *Construction and Building Materials*, 356, p. 129058.

[11] Tang, P., Mo, L., Pan, C., Fang, H., Javilla, B. and Riara, M., 2018. Investigation of rheological properties of light colored synthetic asphalt binders containing different polymer modifiers. *Construction and Building Materials*, 161, pp. 175–185.

[12] Martínez-Boza, F., Partal, P., Conde, B. and Gallegos, C., 2000. Influence of Temperature and Composition on the Linear Viscoelastic Properties of Synthetic Binders. *Energy & Fuels,* 14 (1), pp. 131–137.

[13] Martínez-Boza, F., Partal, P., Conde, B. and Gallegos, C., 2001. Steady-state flow behaviour of synthetic binders. *Fuel*, 80 (3), pp. 357–365.

[14] Navarro, F.J., Partal, P., Martínez-Boza, F. and Gallegos, C., 2005. Effect of composition and processing on the linear viscoelasticity of synthetic binders. *European Polymer Journal*, 41 (6), pp. 1429–1438.

[15] Sun, M., Zheng, M., Qu, G., Yuan, K., Bi, Y. and Wang, J., 2018. Performance of polyurethane modified asphalt and its mixtures. *Construction and Building Materials*, 191, pp. 386–397.

[16] Deng, M., Ding, Y., He, Z., Shan, B., Cao, X. and Tang, B., 2021. Investigation on performances and nano-adhesion behavior of ultra-thin wearing course using polyurethane as binder. *Construction and Building Materials,* 278, p. 122349.

[17] Kaurase, K.P. and Singh, D., 2020. Delonix Regia Fruit Fibers: A New Potential Source of Cellulosic Fibers. *Materials Science Forum*, 979, pp. 185–196.

[18] Kaurase, K.P. and Singh, D., 2020. Investigation on Chemical Isolation and Characterization of Cellulose from Delonix regia Fruit Fibers. *Trends in Manufacturing and Engineering Management: Select Proceedings of ICMechD*, 2019, pp. 303–314.

[19] Kaurase, K.P. and Singh, D., 2024. Influence of Filler Content on the Mechanical, Thermal, Moisture Absorption, and Biodegradability Properties of Bionanocomposite with Cellulosic Fibers Derived from Delonix Regia Fruits. *Mechanics of Advanced Composite Structures*, 11 (1), pp. 73–86.

[20] Kaurase, K.P. and Singh, D., 2022. Isolation of Cellulosic Nano Fibers from Delonix Regia Fruits by Mechano-chemical Route. *International Journal of Vehicle Structures and Systems*, 14 (4), pp. 518-523.

[21] Deng, M., Cao, X., He, Z., Wei, K. and Tang, B., 2023. Experimental and molecular dynamics simulation investigation on filler reinforcement for property enhancement of PU composites. *Mechanics of Advanced Materials and Structures*, 30 (13), pp. 2780–2792.

[22] Gao, X., Zhou, B., Guo, Y., Zhu, Y., Chen, X., Zheng, Y., Gao, W., Ma, X. and Wang, Z., 2010. Synthesis and characterization of well-

dispersed polyurethane/CaCO3 nanocomposites. *Colloids and Surfaces A: Physicochemical and Engineering Aspects*, 371(1-3), pp. 1-7.

[23] Bocci, M., Grilli, A., Cardone, F. and Virgili, A., 2012. Clear Asphalt Mixture for Wearing Course in Tunnels: Experimental Application in the Province of Bolzano. *Procedia-Social and Behavioral Sciences*, 53, pp.115-124..

[24] Bocci, E. and Bocci, M., 2014. Clear asphalt concrete for energy saving in road tunnels. *In Proceedings of the 12th International Conference on Asphalt Pavements (ISAP)*, 2, pp. 1817-1825.

[25] Munera, J.C. and Ossa, E.A., 2014. Polymer modified bitumen: Optimization and selection. *Materials & Design (1980-2015)*, 62, pp. 91-97.

[26] Xin, Z.G., 2014. Research Application of Colored Asphalt Mixture Pavement. Advanced materials research, 900, pp. 459-462.

[27] De Tang, X., Kong, C., Tian, J., Li, Y., Jin, Z.T. and Bai, H.Y., 2015. Preparation and Pavement Performance of Colored Asphalt. *Applied Mechanics and Materials*, 727, pp. 362-365.

[28] Lee, H. and Kim, Y., 2007. Laboratory Evaluation of Color Polymer Concrete Pavement with Synthetic Resin Binder for Exclusive Bus Lanes. *Transportation Research Record: Journal of the Transportation Research Board*, 1991(1), pp. 124-132.

[29] Liu, Z., Wei, K., Wang, S., Ma, B., Wang, X., Shi, W. and Xu, J., 2021. Effect of high-temperature-resistant epoxy resin/polyethylene glycol 2000 composite stereotyped phase change material particles on asphalt properties. *Construction and Building Materials*, 300, p. 124007.

[30] Kalaee, M., Akhlaghi, S., Nouri, A., Mazinani, S., Mortezaei, M., Afshari, M., Mostafanezhad, D., Allahbakhsh, A., Dehaghi, H.A., Amirsadri, A. and Gohari, D.P., Effect of nano-sized calcium carbonate on cure kinetics and properties of polyester/epoxy blend powder coatings. *Progress in Organic Coatings*, 71(2), pp. 173-180..

[31] de Moura, A.P., da Silva, E.H., dos Santos, V.S. , Galera, M.F., Sales, F.C., Elizario, S., de Moura, M.R., Rigo, V.A. and da Costa, R.R., 2021. Structural and mechanical characterization of polyurethane-CaCO 3 composites synthesized at high calcium carbonate loading: An experimental and theoretical study. *Journal of Composite Materials*, 55(21), pp. 2857-2866.

[32] J. Donate-Robles, J. and Martín-Martínez, J.M., 2011. Addition of precipitated calcium carbonate filler to thermoplastic polyurethane adhesives. *International Journal of Adhesion and Adhesives*, 31(8), pp. 795-804..

[33] Al Omari, M.M.H., Rashid, I.S., Qinna, N.A., Jaber, A.M. and Badwan, A.A., 2016. Chapter Two - Calcium Carbonate. Editor(s): Harry G. Brittain, Profiles of Drug Substances, Excipients and Related Methodology. *Academic Press*, 41, pp. 31-132,

[34] Du, Y., Liu, P., Wang, J., Wang, H., Hu, S., Tian, J. and Li, Y., 2019. Laboratory investigation of phase change effect of polyethylene glycolon on asphalt binder and mixture performance. *Construction and Building Materials*, 212, pp. 1-9.

[35] Wang, Q., Min, Z., Cheng, L., Zhang, Y., Sun, J., Wong, Y. D. and Shao, K., 2024. An epoxy asphalt with polyethylene glycol chains for porous mixtures containing reclaimed asphalt pavement. *Case Studies in Construction Materials*, 20, p. e02972.

[36] Kaurase, K. P. and Singh, D., 2023. Mechanical and Barrier Properties of Cellulosic Nano-Fibers Reinforced Bionanocomposite. *International Journal of Vehicle Structures & Systems (IJVSS)*, 15(1).